九州大学大学院総合理工学府報告
第 37 巻 第 2 号 19-26 頁 平成 28 年 2 月

Engineering Sciences Reports, Kyushu University
Vol. 37, No. 2, pp. 19-26, FEB., 2016

An experimental study on aerodynamic interaction between a boundary layer generated by a smooth and rough wall and a wake behind a spire

Nurizzatul Atikha RAHMAT*1,2†, Aya HAGISHIMA*3, Naoki IKEGAYA*3, Jun TANIMOTO*3

†E-mail of corresponding author: ezatikha@gmail.com

(Received January 22, 2016, accepted January 25, 2016)

A wind tunnel experiment to assess the flow characteristics of the wake behind a spire mounted normal to the wind tunnel floor was conducted to clarify the interaction between the wake flow and the wall shear boundary layer. To reproduce the contrasting boundary layer depth, two types of walls—a smooth wall and a regular cube array—were adopted; for each wall, the spanwise distribution of the streamwise velocity was measured at two downwind positions and seven heights within and above the wall boundary layer with and without a spire. The spanwise distribution of the wake generated by the spire far above the wall boundary layer with low turbulence agreed with the well-known function for two-dimensional (2D) wake flow, derived theoretically from the gradient-diffusion model, despite the weak asymmetry of the inflow. In contrast, the spanwise distribution of the wake within or near the outer edge of the wall boundary layer showed different trends from that of the 2D wake flow. In the former, the expansion of the wake width is compressed in the lateral direction by the turbulence of the wall boundary layer and the velocity deficit of the wake is sustained far from the spire.

Key words: *Wind tunnel, spire, wake flow, wall shear boundary layer*

1. Introduction

The flow field around a building has been an important research target in the wind engineering field over the last half-century for robust structural design and the safety of pedestrians (e.g. Hunt[1]). In particular, flow around a slender tall building or long structures such as cables can be categorized as widely observed typical flow around a two-dimensional bluff body in a free turbulent flow, which has been one of the primary research areas of fluid dynamics for a century (e.g. Townsend[2], Taneda[3], and Hunt[4]).

In contrast, for the past few decades, intensive studies on the aerodynamic nature of the urban boundary layer have been also conducted for better prediction of the urban climate. From a climatological viewpoint, the urban atmosphere has been considered as a boundary layer over a fully rough wall[5] which consists of several layers, including a roughness sublayer and an inertial sublayer (e.g. Rotach et al.[6]). Within the inertial sublayer, vertical profiles of environmental variables such as velocity have been known to satisfy the similarity theory characterized by several aerodynamic parameters including the roughness length and displacement height, which depend on urban geometry[7]. A series of our recent experimental work (e.g. Hagishima et al.[8]) has been motivated by the interest in the relation between urban geometry and these aerodynamic parameters. In the course of these experiments, the authors encountered an interesting phenomenon related to the aerodynamic interaction between the previously mentioned two types of flow, namely, wakes behind a row of spires installed at the upwind of a wind tunnel and a rough wall boundary layer developing over a block array. The original reason for installing spires was to produce large-scale turbulence similar to natural atmospheric boundary layer having sufficient depth even with the limitation of short streamwise length of wind tunnels[9].

Meanwhile, several previous studies have investigated the characteristics of flows that simultaneously involve both boundary layers and wakes behind spires. Counihan[10] measured the distribution of the velocity defect behind a 2D surface obstacle whose height is assumed to be smaller than the boundary layer height (BLH, or alternatively, δ). On the contrary, Castro[11] studied the

*1 Universiti Malaysia Pahang (UMP)
*2 Department of Energy and Environmental Engineering, Graduate student
*3 Department of Energy and Environmental Engineering

recovery of the boundary layer in the wake of a two-dimensional surface-mounted obstacle. However, these studies were mainly focused on the vertical structure of the turbulent boundary layer, yet the flow structure in a lateral distribution is rarely reported.

With this background, this paper presents the results of a wind tunnel experiment on modifications in the wake flow behind a spire because of interaction with the wall boundary layer.

2. Experimental setup

2.1 Wind tunnel device

The experiment was conducted in a closed return wind tunnel at the laboratory of the Interdisciplinary Graduate School of Engineering Sciences, Kyushu University, Japan. The wind tunnel has a working section 1 m high × 1.5 m wide with a streamwise length of 8 m. The spatial uniformity of the inflow condition was carefully adjusted by means of a honeycomb layer of 10 mm hexagonal cells with a loss coefficient of 0.2 and 9 layers of mesh screens with an open-area ratio larger than 0.57. The placement of the mesh screens was determined by a trial and error method employed in a preliminary experiment and by referring to previous experimental work by Mehta[12].

2.2 Measurement conditions

In the experiment, a quasi-quarter elliptic spire shown in Figs. 1(a) to 1(f) with a height of 0.8 m, which is higher than the wall boundary layer, was adopted as an obstacle for generating the wake flow. The depth of the spire is 0.04 m (hereafter, W_S) up to a vertical height of 0.25 m.

The spire was installed in the upwind centre position of the wind tunnel floor, and the distributions of the streamwise velocity behind the spire were measured at two leeward positions: namely, the near wake region A (an area just behind the spire) and the far wake region B as shown in Fig. 2.

Two types of floors (to obtain contrasting boundary layer depth) were used in the wind tunnel for generating the turbulent shear boundary layer: the first one was a smooth surface where flat plastic plates covered the floor of the wind tunnel with a streamwise length of about 3.4 m, and the other was a rough wall consisting of a staggered cubical array with a height of 25 mm (hereafter, H) and a packing density λ_p of 17.4%. The streamwise length of the smooth wall and the block array was about 136 H and 85 W_S.

2.3 Instrumentation and measurement positions

The vertical distribution of the streamwise velocity was measured on a laterally centred point at the two positions A and B for both the smooth and rough wall conditions without a spire. The measurement heights were from 0.5 H to 20 H with an interval of 0.1 H. Based on these measurements, the boundary layer height for each position was determined as described in section 3.1.

In addition, the lateral distribution of the streamwise velocity at positions A and B were measured with and without a spire at seven elevations including both below and above the BLH. The measurement heights below the BLH range from 0.25 δ to 1.25 δ with an interval of 0.25 δ; 15 H and 20 H were adopted

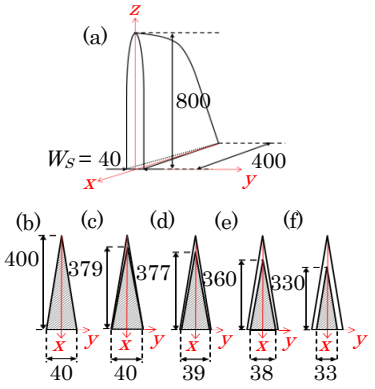

Fig. 1. (a) Schematic figure of a spire and its dimensions; top view of the spire base (wedge-shaped) showing vertically different widths ((b) z = 0; (c) z = 250 mm; (d) z = 275 mm; (e) z = 375 mm; (f) z = 500 mm). All units in mm.

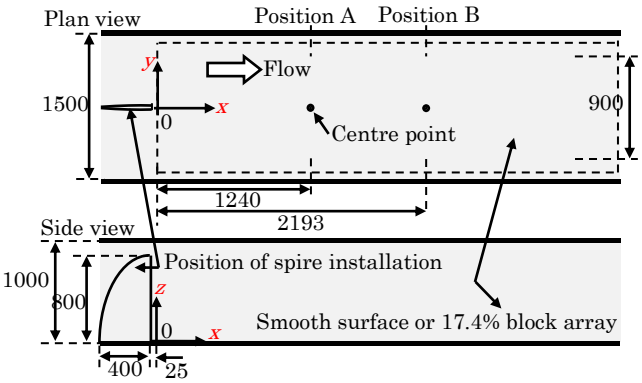

Fig. 2. Schematic figure of test section and measurement positions. All units in mm.

as the heights above the BLH. The spatial resolution of the measurement in the spanwise direction was 5 mm (= 0.2 H) for the range of $-14\ H < y < 14\ H$ and 10 mm (= 0.4 H) for the range of both $-18\ H < y < -14\ H$ and $14\ H < y < 18\ H$, and the total number of measurement points in the lateral line was 162.

The streamwise velocity was measured using a split-film anemometer (Dantec Dynamics, 55R55), which was placed at each measurement position by a 3D auto traverse system. The measurements were performed with a reference stream velocity of approximately 8 ms^{-1}. The reference stream velocity (x, $y = 0$, $z = 20\ H$) was measured at each lateral path to check the time variation of the sensitivity of the hot-wire anemometer. The measurement frequency and period were 1000 Hz and 30 s, and the data were recorded using a CTA unit (Kanomax, Model 1101) and a data logger (Graphtec, GL900). The calibration of the hot-wire anemometer was performed at least every 24 h using a pitot tube.

3. Results and discussion

3.1 Vertical profiles of velocity for the smooth and rough surfaces without a spire

Fig. 3 shows the vertical profiles of the mean, standard deviation, and skewness of the streamwise velocity at the lateral central point ($y = 0$) of positions A and B for both wall conditions without a spire. The mean wind profiles over the smooth and rough surfaces shown in Figs. 3(a) and 3(b) exhibit a clear change in the velocity gradient at heights of around 3 H and 5 H, respectively, and the velocities above these heights are almost constant for both conditions. This difference of height between the smooth surface and the block array is due to the difference in surface drag. In addition, the height at which the change in the velocity gradient occurs increases with an increase in the streamwise distance from A to B owing to the development of a boundary layer.

With regard to the standard deviation, the data for the smooth wall case show the highest values at the lowest measurement height, and the values gradually decrease with the height. In contrast, the values for the rough wall case exhibit a peak at a height of around 1 H because of the block array. The height where the standard deviation is about 1% in the smooth case is lower than that in the rough case, and it increases in the order of the streamwise position because of the boundary layer development.

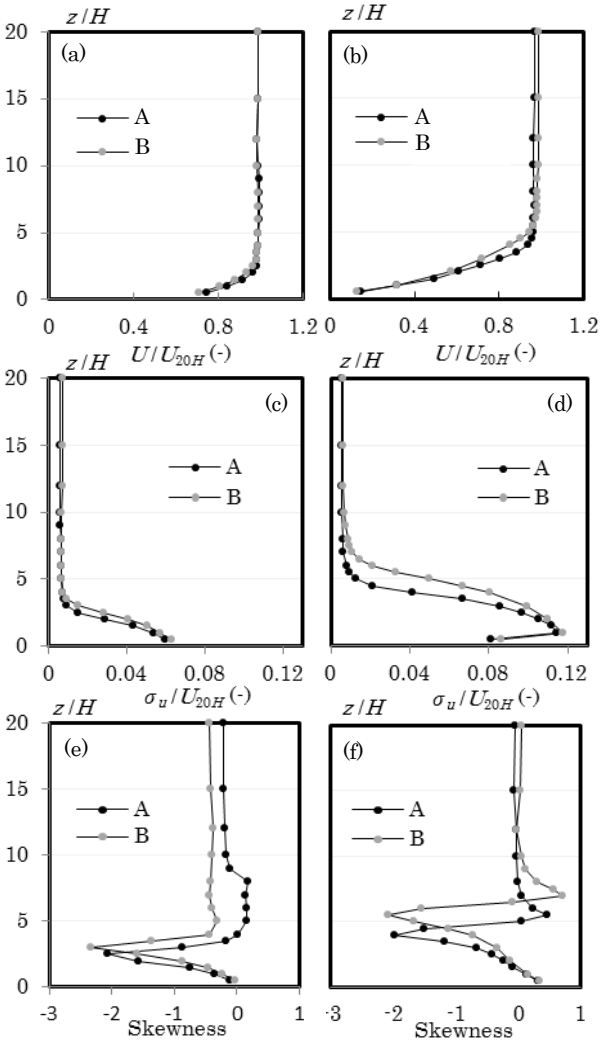

Fig. 3. Vertical velocity profiles for the mean direction over both surface conditions at the centre point of A and B for smooth surface: (a) normalized mean velocity, (c) turbulence intensity, and (e) skewness of U; for rough surface with a staggered cubical array with $\lambda_P = 17.4\%$: (b) normalized mean velocity, (d) turbulence intensity, and (f) skewness of U.

Table 1 Boundary layer height determined based on a negative peak of skewness of streamwise velocity under cases without a spire.

Streamwise position	A	B
Smooth surface	60.0mm (2.4 H)	77.5mm (3.1 H)
Rough surface	103mm (4.1 H)	138mm (5.5 H)

In contrast, as shown in Figs. 3(e) and 3(f), the skewness of the streamwise velocity near the surface decreases with the height, shows a

sharp negative peak, and returns to around zero for both conditions. This trend is consistent with previous experimental data by Raupach[13]. By comparing the profiles of the skewness with those of the mean wind, we can see that the height of the negative peak in the skewness profiles is consistent with the height at which the mean velocity becomes almost independent of the height.

Considering the fact that the mean wind profile far above the wind tunnel floor shows a weak height dependency, it is difficult to accurately determine the 99% boundary layer height. Hence, we treated the height of the negative sharp peak of the skewness profile as the BLH δ for the following analysis. Table 1 summarizes the BLH determined at each position for all cases.

3.2 Spanwise distributions of velocity

Fig. 4 presents the velocity distributions in the spanwise direction for the smooth and rough surfaces with and without a spire at position B for several chosen heights. The velocity is normalized by Eq. (1) as follows.

$$U_n(x,y,z) = U(x,y,z)/U(x,y=-18H,z=20H) \quad (1)$$

The reference position of the normalization is at $y = -18$ H, $z = 20$ H, where the influence of the spire should be minimal. As shown in Fig. 4(a), the velocity profile for the smooth case without a spire at 20 H (far above the boundary layer) is almost laterally constant with a relative standard deviation of 0.7%. However, the profiles measured inside the boundary layer (0.25 δ and 0.5 δ) show negatively sloped curves with a larger relative standard deviation of 0.8%.

The profiles of the smooth case with a spire show a clear effect of the wake of the spire, as expected. A negative peak in velocity due to the spire can be seen at $y = 0$ for the heights 0.25 δ and 0.5 δ, and two positive peaks can be observed at $y = \pm 6$ H for these heights. With regard to the data far above the wall boundary layer, the position of maximum velocity deficit is slightly shifted in the negative y direction from the position of the spire ($y = 0$), and there is no positive peak. The trend for the rough surface case, shown in Fig. 4(b), is almost similar to that for the smooth case; however, the profile of the case without a spire at 0.25 δ and 0.5 δ show a larger relative standard deviation of 1.9% and 1.1%, respectively, compared with that of the smooth condition.

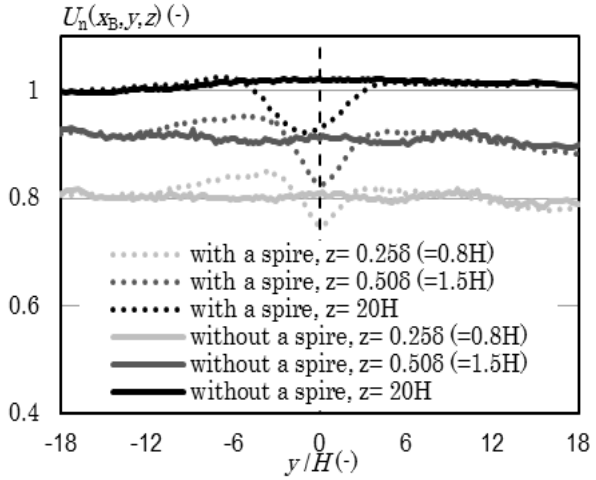

(a) Smooth surface

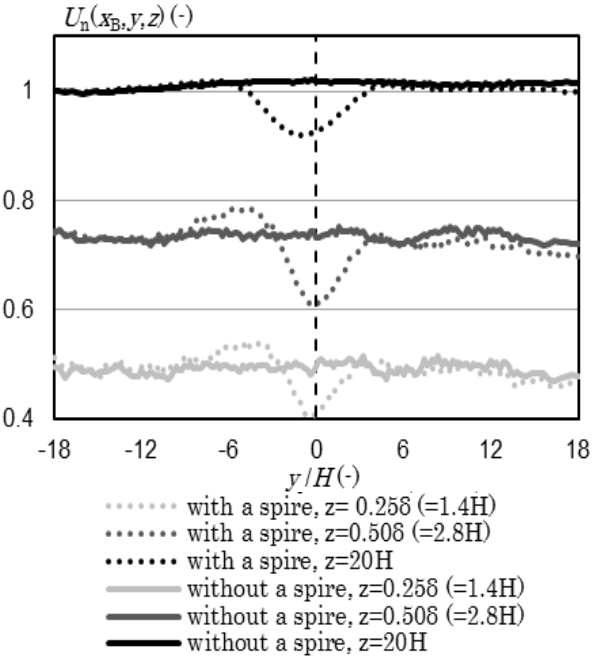

(b) Rough surface

Fig. 4. Spanwise distribution of velocity at B ($x = 87.7$ H)

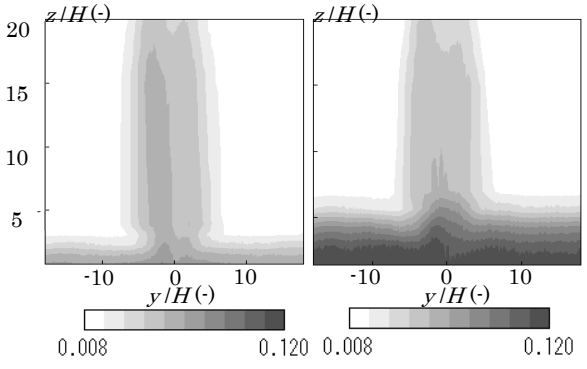

(a) Smooth surface (b) Rough surface

Fig. 5. Contours of the standard deviation $\sigma_U(x, y = -18$ H, $z = 20$ H) of the streamwise velocity for the cases with a spire at B ($x = 87.7$ H).

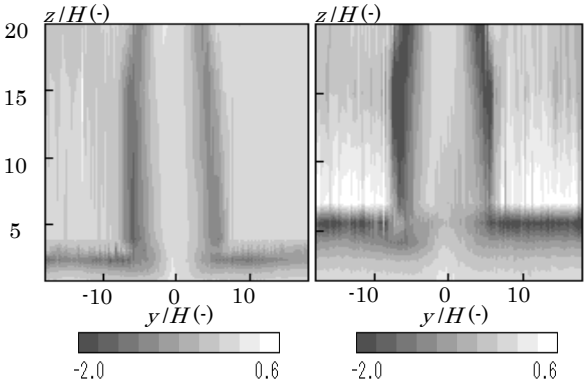

(a) Smooth surface　　(b) Rough surface

Fig. 6. Contours of the skewness of the streamwise velocity by the spire at B (x = 87.7 H).

The spatial distributions of the standard deviation and skewness of the streamwise velocity in the lateral-vertical plane at position B for the smooth and rough cases with a spire are shown in Figs. 5 and 6, respectively. The standard deviation of both cases monotonically increases as the position approaches both the floor and region behind the spire, and dark-coloured regions show weak asymmetric patterns. On the contrary, Fig. 6 indicates that the wake of the spire and the wall boundary layer are rimmed with dark colored regions with strongly negative skewness of around −1.6 to −2.0.

3.3 Spanwise variations of the velocity deficit

The 2D wake in a free shear layer is widely characterized by the velocity deficit, which is the velocity difference between the background and wake regions. However, considering the non-uniformity of the inflow conditions of the present experiment as shown in Fig. 4, for the following analysis, we adopted the difference in the normalized velocity between experiments with and without a spire as the velocity deficit, which is expressed by Eq. (2).

$$\Delta U_n = U_n^{NS}(x,y,z) - U_n^{S}(x,y,z) \qquad (2),$$

where superscripts S and NS refer to values for the cases with and without a spire, respectively. Fig. 7 shows the spanwise distributions of the velocity deficit ΔU_n defined by Eq. (2) at positions A and B for the smooth condition.

As can be seen from the result at position A (Fig. 7(a)), ΔU_n for heights above the BLH, such as 1.23 δ (= 3.0 H), 15 H, and 20 H, shows a positive peak. However, its position is slightly shifted from right behind the spire to the negative y direction (y = −0.8 H, at a height of 20 H), and gradually decreases along both lateral directions. This trend is almost similar to the well-known wake flow behind a bluff body (e.g. Schobeiri[14]). The maximum velocity deficit at around y = 0 decreases with the decrease of the height. In addition, ΔU_n does not completely converge to zero even at the furthermost positions (y = 18 H), possibly due to the non-uniformity of the inflow other than by the spire. In contrast, positive peaks at around y = 0 for the other four heights lower than the BLH are much smaller than those above the BLH. Furthermore, two negative peaks can be observed at y = ±4 H, and these accelerated velocities gradually recover with increasing lateral distance from y = 0. Although such distribution patterns might be partially caused by the asymmetric inflow of the wind tunnel, it is obvious that the spanwise profiles of ΔU_n below the BLH are much different from those far above the BLH.

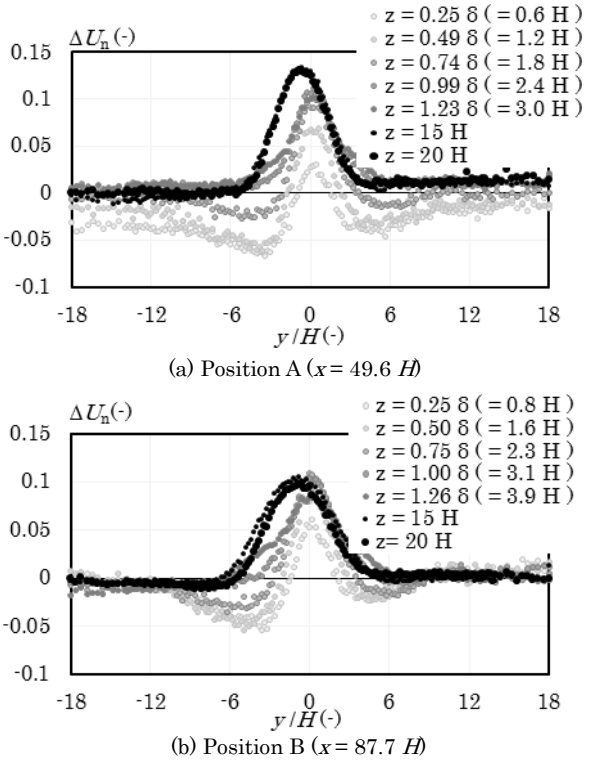

(a) Position A (x = 49.6 H)

(b) Position B (x = 87.7 H)

Fig. 7. Velocity deficit by the spire for smooth surfaces.

On the contrary, at position B (Fig. 7(b)), positive peaks in ΔU_n near y = 0 at heights above the BLH (15 H and 20 H) are about 23% smaller compared to those at position A, and the changes in the slopes of the distributions are more gradual. Such a tendency in the recovery of the velocity deficit according to the streamwise distance is a common feature of

wake flow. In contrast, the values of the positive peaks for the other five heights from 0.25 δ to 1.25 δ are almost the same as those at position A. In other words, the velocity deficit, due to the spire, far above the BLH with low turbulence gradually recovers as the streamwise distance increases, whereas that within the wall shear boundary layer with high turbulence is sustained far away from the spire.

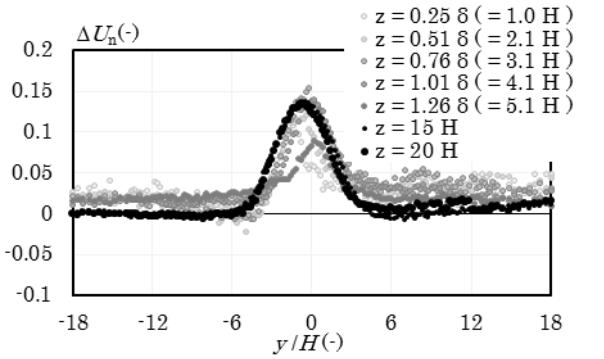

(a) Position A (x = 49.6 H)

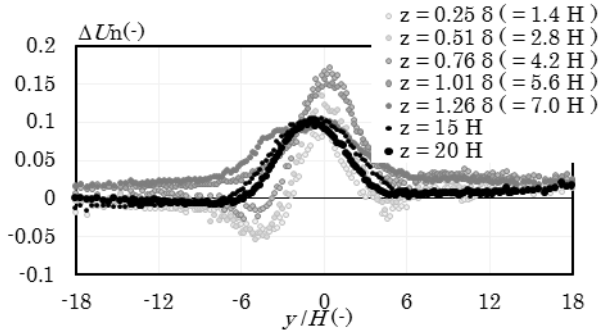

(b) Position B (x = 87.7 H)

Fig. 8. Velocity deficit by the spire for rough surfaces.

The velocity deficit of the rough surface case, shown in Fig. 8, is almost consistent with the above-mentioned tendency for the smooth case. The distributions of ΔU_n far above the BLH for the rough case exhibit a positive peak near y = 0, and the deficit becomes mild at the downward position B compared with position A, similar to the smooth surface condition. However, the velocity deficit profiles of the rough surface case are significantly higher than the corresponding profiles for the smooth surface case, probably due to the underlying blocks and its canopy flow, which hinder the development of a wake. Similar results were reported for shallow turbulent wakes generated on smooth and rough surfaces by Tachie and Balachandar[15].

With regard to the rough case below the BLH at position A (Fig. 8(a)), ΔU_n at $y = \pm 18$ H appears to be positive in contrast to the data of the smooth surface case (Figs. 7(a) and 7(b)) and downward position B of the rough surface case (Fig. 8(b)). Furthermore, at downwind position B (Fig. 8(b)), the acceleration of velocity below the BLH at around $y = \pm 6$ H is evident compared to position A (Fig. 8(a)). Although determining the precise reason for this tendency is difficult due to the non-uniformity of the inflow condition, the installation of the spire might be a cause for the flow acceleration[15].

It is known that the velocity deficit due to a 2D obstacle in a free shear flow can be expressed by a self-similar general function based on the gradient-diffusion model[16] as follows:

$$g(y/y_{0.5}) = \exp(-\alpha (y/y_{0.5})^2) \quad (3),$$

where α is an empirical constant and $y_{0.5}$ is the half wake width.

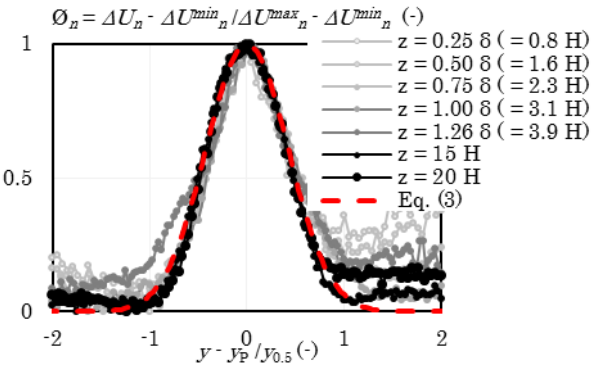

(a) Smooth surface

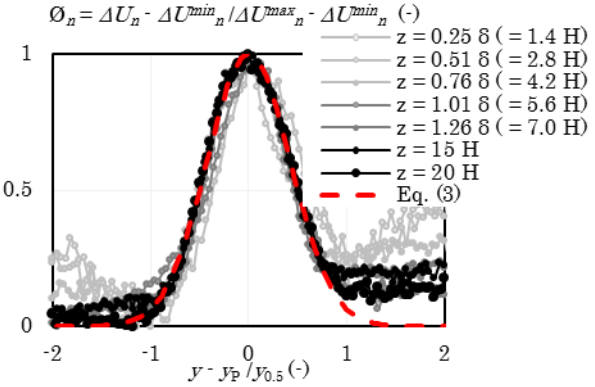

(b) Rough surface

Fig. 9. Normalized velocity deficit by the spire at position B (x = 87.7 H).

Fig. 9 shows a comparison of the spanwise distributions of the velocity obtained by this equation and that obtained by the measurements at position B. The constant α,

included in Eq. (3), was determined to be 2.76 and 2.68 for the smooth and rough cases, respectively, based on the measured data at 20 *H*. As previously mentioned, the spanwise profiles of the velocity deficit, shown in Figs. 7 and 8, are not perfectly symmetric. Thus, in the vertical axis of Fig. 9, the velocity deficit ΔU_n is reduced by the minimum value of ΔU_n in the lateral measurement line (hereafter, $\Delta U^{min}{}_n$), and normalized by the value ($\Delta U^{max}{}_n$ - $\Delta U^{min}{}_n$), where $\Delta U^{max}{}_n$ is the maximum value of ΔU_n in the lateral measurement line. Henceforth, we refer to ($\Delta U^{max}{}_n - \Delta U^{min}{}_n$) as the normalized maximum velocity deficit for simplicity. The horizontal axis is the spanwise distance normalized by the half wake width $y_{0.5}$. $y_{0.5}$ is determined by the distance between two positions where $\Delta U_n = 0.5(\Delta U^{max}{}_n - \Delta U^{min}{}_n)$, in accordance with the vertical axis. Because of the slightly heterogeneous inflow condition, the origin of the spanwise direction was shifted by y_P to align the peak of $(\Delta U_n - \Delta U^{min}{}_n)/(\Delta U^{max}{}_n - \Delta U^{min}{}_n)$ with the coordinate origin.

The data for both surface conditions at the heights of 15 *H* and 20 *H* agree with the estimations from Eq. (3), except for the slight discrepancy at $|(y - y_P)/y_{0.5}| > 1$, where it does not coincide with 0. This indicates that in the present experiment the flow structure far above the wall boundary layer can be categorized as a typical 2D wake of a bluff body in a free stream in spite of the non-uniform inflow condition. On the contrary, the normalized profiles of all heights below 1.25 δ show significant departure from Eq. (3). In particular, the data at 0.25 δ, 0.5 δ, and 0.75 δ show remarkably different trends from the accelerated velocity at $|(y - y_P)/y_{0.5}| > 0.5$. Although it is not certain whether such flow acceleration is caused by either the asymmetrical lateral distribution of the inflow or the interaction between the wake and the wall boundary layer, the discrepancy of the flow field within and above the BLH is evident.

3.4 Vertical distributions of the maximum velocity deficit and half wake width

Fig. 10 indicates how vertical distributions of the normalized maximum velocity deficit are modified with the change of streamwise distance. The vertical axis is the height normalized by the BLH at each streamwise position.

The normalized maximum velocity deficit increases with height from near the floor, shows a steep positive peak around a height of 0.75 δ, and rapidly reduces up to a height of 1.25 δ for all positions. With regard to the data above the wall boundary layer, the normalized maximum velocity deficit drastically increases with the height. In addition, for both surface conditions, the normalized maximum velocity deficit above a height of 1.25 δ clearly shows a decrease with the streamwise distance, and this is the well-known recovery process of the wake in a free shear flow. In contrast, the data below the wall boundary layer indicate that the maximum deficit increases from position A to downwind position B.

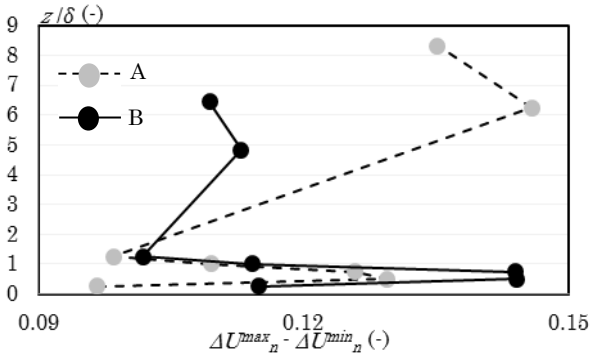

(a) Smooth surface

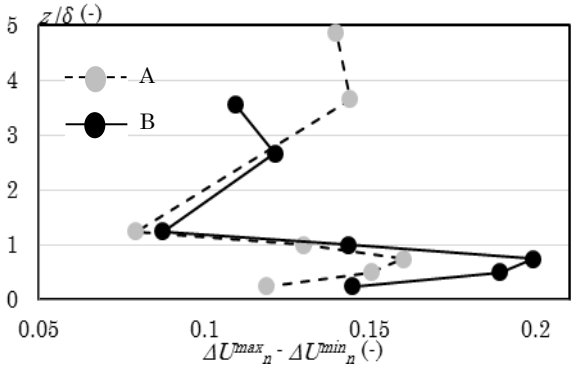

(b) Rough surface

Fig. 10. Change of the maximum velocity deficit with respect to height.

The data of the half-wake width are shown in Fig. 11 in the same manner as Fig. 10. For both surface conditions, the data of the half-wake width above the BLH at position B is larger than the corresponding data at position A. Furthermore, the data of the half-wake width increase with the height from near the floor, show a small peak at the heights of 1.00 δ and 0.76 δ for smooth and rough surfaces, respectively, then slightly decrease at around BLH (Fig. 11(b)), and finally rapidly increase above BLH. It is noteworthy that the half-wake width within

the wall boundary layer is much smaller than that above the BLH. In other words, the expansion of the wake in the lateral direction behind a slender obstacle is compressed in the lateral direction by the underlying wall surface and wall boundary turbulence, and consequently, the velocity deficit of the wake becomes steep compared to the ordinary 2D wake flow in a free shear flow.

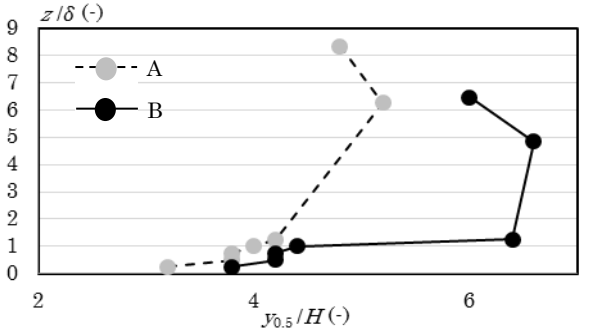

(a) Smooth surface

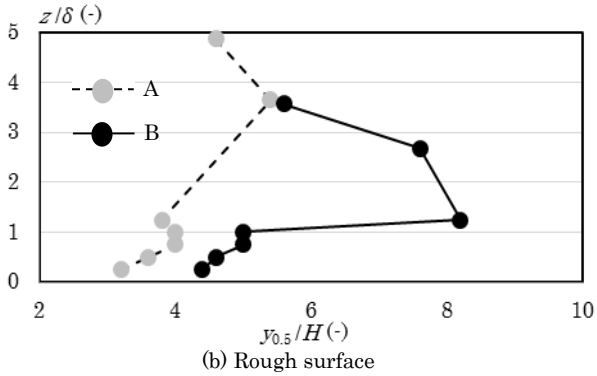

(b) Rough surface

Fig. 11. Change of the half wake width $y_{0.5}$ with respect to height.

4. Conclusions

The present study was designed to investigate the aerodynamic interaction between the wall shear boundary layer and the wake flow generated downwind of an isolated slender obstacle normal to the wall. The detailed measurements of the distributions of the streamwise velocity above the smooth and rough wall surfaces, with and without a spire, were conducted in a wind tunnel. The spanwise variations of the velocity behind a spire above the wall boundary layer show good agreement with the 2D self-similar profile for a 2D wake flow in a free shear flow, despite the weak asymmetrical inflow condition of the wind tunnel. In contrast, the spanwise profiles of the velocity within the wall boundary layer show clear discrepancies from the 2D wake flow: the expansion of the wake width in the lateral direction is compressed, and the velocity deficit within the wake region is more significant compared with the data above the wall boundary layer. Although the present experimental data indicate an obvious difference in the profiles of the wake flow within and above the wall boundary layer, a detailed understanding of the features of these differences has not been completely attained because of certain limitations mainly caused by the non-uniform inflow condition of the wind tunnel. The turbulent statistics of not only the streamwise velocity component, but also the lateral component would be essential for elucidating the mechanism of the interference of the spanwise expansion of the wake due to the wall boundary turbulence, and will be one of our future tasks.

References

1) Hunt, J. C. R. The effect of single buildings and structures. Phil. Trans. Roy. Soc., A, 269, 457–467 (1971).
2) Townsend, A. A. Momentum and energy diffusion in the turbulent wake of a cylinder. Proc. Roy. Soc. (London), A, 197, 124–140 (1949).
3) Taneda, S. Downstream development of wakes behind cylinders. J. Phys. Soc. Jpn., 14, 843–848 (1959).
4) Hunt, J. C. R. A theory of turbulent flow round two-dimensional bluff bodies. J. Fluid Mech., 61, 625–706 (1973).
5) Townsend, A. A. The structure of turbulent shear flow, 2nd ed., Cambridge University Press, 554–560 (1976).
6) Rotach, M. W., et al. BUBBLE – an urban boundary layer meteorology project. Theor. Appl, Climatol., 81, 231–261 (2005).
7) Grimmond, C. S. B., Oke, T. R. Aerodynamic properties of urban areas derived from analysis of surface form. J. Appl. Meteor., 38, 1262–1292 (1999).
8) Hagishima, A., et al. Aerodynamic parameters of regular arrays of rectangular blocks with various geometries. Boundary Layer Meteorol., 132, 315–337 (2009).
9) Counihan, J. An improved method of simulating an atmospheric boundary layer in a wind tunnel. Atmos. Environ., 3, 197–214 (1969).
10) Counihan, J. Wakes behind two-dimensional surface obstacles in turbulent boundary layers. J. Fluids Eng., 64, 529–563 (1974).
11) Castro, I. P. Relaxing wakes behind surface-mounted obstacles in rough wall boundary layers. J. Fluid Mech., 93, 631–659 (1979).
12) Mehta, R. D. Turbulent boundary layer perturbed by a screen. AIAA J., 23, 1335–1342 (1985).
13) Raupach, M. R. Conditional statistics of Reynolds stress in rough-wall and smooth-wall turbulent boundary layers. J. Fluid Mech., 108, 363–382 (1981).
14) Schobeiri, M. T. Fluid mechanics for engineers, Springer, 340–351 (2010).
15) Tachie, M. F., Balachandar, R. Shallow wakes generated on smooth and rough surfaces. Experiments in Fluids, 20, 467–474 (2001).
16) Schlichting, H., Gersten, K. Boundary layer theory. 8th ed., Springer (2000).